IEEE Access
Multidisciplinary | Rapid Review | Open Access Journal

Received 7 September 2022, accepted 24 September 2022, date of publication 30 September 2022,
date of current version 11 October 2022.

Digital Object Identifier 10.1109/ACCESS.2022.3210981

RESEARCH ARTICLE

Hybrid Particle Swarm Optimization–Gravitational Search Algorithm Based Detection of Graphene Defects With Electrical Impedance Tomography

SUNAM KUMAR SHARMA, ANIL KUMAR KHAMBAMPATI, AND KYUNG YOUN KIM
Department of Electronic Engineering, Jeju National University, Jeju 63243, South Korea

Corresponding author: Kyung Youn Kim (kyungyk@jejunu.ac.kr)

This work was supported by the Mid-Career Researcher Program through the National Research Foundation of Korea (NRF) Grant funded by the Korean Government (MSIP; Ministry of Science, ICT & Future Planning) under Grant NRF-2020R1A2C2006463 and by the Basic Science Research Program through the National Research Foundation of Korea (NRF) funded by the Ministry of Education (2022R1I1A3053600).

ABSTRACT Recently, graphene has gained a lot of attention in the electronic industry due to its unique properties and to overcome the limits of miniaturization making way for novel devices in the field of electronics. Among the synthesizing methods for growing large graphene films, chemical vapour deposition is one of the promising and common techniques but defects such as cracks, holes, or wrinkles are hard to avoid. The presence of defects influence the electrical properties of graphene thus the local conductivity distribution across the surface of the graphene can characterize its electrical behavior. The difference in conductivity values of the defect and the background can be estimated with electrical impedance tomography. Due to the very high conductivity of graphene, the reconstructed electrical impedance tomography conductivity images suffer from poor spatial resolution. Considering the graphene defect conductivity and the number of defects are known a priori then the unknowns are defect geometry and background conductivity of graphene that are estimated using hybrid particle swarm optimization - gravitational search algorithm. The defect geometries are described by truncated Fourier series coefficient which can represent the complex shapes. Numerical studies are done for graphene characterization with single and multiple defects. Monte Carlo simulations with 20 runs having different noise seed are carried out to evaluate the robustness of the proposed algorithm. Statistical analysis is done and the results of the proposed algorithm are compared against the conventional modified Newton Raphson method and gravitational search algorithm. Experimental studies with graphene sheet 2.5 cm $\times$ 2.5 cm with defects are performed for shape estimation. The results showed that the proposed algorithm has a good estimation of background conductivity and defect geometry.

INDEX TERMS Graphene, parameter estimation, EIT, PSOGSA, defect detection.

NOMENCLATURE

ERT	Electrical resistance tomography
EIT	Electrical impedance tomography
mNR	Modified Newton-Rapshon
GSA	Gravitational search algorithm
PSO	Particle swarm optimization
PSOGSA	Particle swarm optimization - Gravitational search algorithm
I_l	Current (mA)
Ω	Domain (object) under study
$\partial\Omega$	Boundary of the object
σ ,$\sigma(P)$	Internal conductivity distribution of the object (mS), $P = (x, y) \in \Omega$
$u(x, y)$	Calculated voltage (mV)
CEM	Control electrode model
e_l	l^{th} electrode, $l = (1, 2, \cdots, L)$
z_l	Contact impedance
V_l	Measured voltage, (mV)
A	Stiffness matrix
B	Solution vector

The associate editor coordinating the review of this manuscript and approving it for publication was Sun-Yuan Hsieh.

This work is licensed under a Creative Commons Attribution 4.0 License. For more information, see https://creativecommons.org/licenses/by/4.0/

f	Data vector
FEM	Finite element method
$Db_n(s)$	Boundary of the n^{th} object, $n = (1, 2, \cdots, N)$
F_ϕ	Order of Fourier series
$\phi_f(s)$	Basis function
$Gamma$	Shape coefficient
$v_i(t)$	Velocity of particle
w	Weighting function
c_k	Weighting factor
a_i	Acceleration of particle
$RMSE$	Root mean square error
Γ	Cost function
$\bar{\lambda}$	Mean of estimated Fourier series coefficient
$M\bar{A}E$	Mean absolute error
$M\bar{E}S$	mean error square
$R\bar{M}SE$	Mean RMSE
E_{sd}	Error standard deviation
λ_t	True Fourier series coefficient
λ	Estimated Fourier series coefficient
mS	MilliSiemens
PMMA	Poly methyl- methacrylate

I. INTRODUCTION

For a long time, the semiconductor industry has been dominated by silicon. But the past few years graphene has gained an enormous scientific interest due to its remarkable electronic [1] properties. Graphene has overcome the limits of miniaturization which is in order of 50nm for the electric channel for silicon-based electronics [2]. Fabrication of graphene is done with several methods such as exfoliation, colloidal suspension, epitaxial growth, chemical vapour deposition (CVD) [3], [4], [5], [6]. However, developing large homogeneous graphene films is very hard and inhomogeneities like wrinkles, holes, and cracks are developed [7].

For realizing and developing graphene based devices, a fast, accurate, nonintrusive method is necessary that can map conductivity distribution for electrical characterization of graphene. Cultera *et al.* [8] used electrical resistance tomography (ERT) to map the conductivity profile of large graphene sheet by placing point electrodes over the boundary and an average gap model is employed as mathematical model. However, this model with point electrodes and does not consider the contact impedance between electrodes and graphene sheet. To overcome this situation, Khambampati *et al.* [9] used a complete electrode model with electrical impedance tomography (EIT) for imaging local conductivity distribution, where EIT is the ac regime equivalent of the ERT. Graphene has very high conductivity value thus the electrode contact impedance does effect the reconstruction performance. Due to ill-posedness, high conductivity of graphene and electrode contact impedance it is very difficult to obtain absolute reconstructions. Therefore in [9] linear difference approach is used to reconstruct the difference estimates. In [10], nonlinear difference imaging approach is used to reconstruct the initial and difference estimates at same time. As seen from previous studies [9], [10], in general, pixel conductivity imaging of graphene suffers from the poor spatial resolution.

The shape estimation is the alternative approach to improve the spatial resolution. In the shape estimation approach the number of unknowns to estimate is less when compared to the conductivity distribution estimation. For this approach a prior information of the conductivity distribution within each closed boundary region is assumed to be known. By this approach we can estimate the shape, size, and location of the defect in the domain. For EIT, the shape of the defect can be defined with various methods such as Fourier series [11], level set [12], front-point [13], B-spline based [14], and supershape [15]. The parameters defining the shape of the defect is estimated by a suitable inverse algorithm. A modified Newton-Rapshon (mNR) algorithm is one of the most used conventional inverse algorithm for estimating shape parameters. However, it shows sub-optimal performance when solving the EIT inverse problem. It heavily depends on the initial guess and Jacobian matrix [16] to find the optimized solution. However, when the shape of the target is complex and mNR tends to produce intersecting boundaries [17]. An algorithm that can converge fast to the optimum solution without the need of Jacobian matrix calculation is preferred. A heuristic algorithm is a good candidate to overcome the Jacobian matrix problem in estimating the complex shape. Particle swarm optimization (PSO), a heuristic algorithm, showed a great exploration capability in estimating the boundary of the elliptic region in EIT domain [18]. Exploitation is the other main characteristic of the heuristic algorithm and the gravitational search algorithm (GSA) has a great exploitation step [19]. GSA estimated the bladder boundary with good accuracy using EIT in the study conducted by the author in [11]. Mirjalili and Hashim [20] introduced a hybrid heuristic algorithm Particle swarm optimization - gravitational search algorithm (PSOGSA) which combined the advantages of PSO and GSA. This new algorithm PSOGSA outperformed the other heuristic algorithms including PSO and GSA. The evaluation of the algorithm was conducted with the standard benchmark functions.

During graphene growth the surface conductivity can change due to operating conditions of CVD process. Graphene is a very high conductive material where the graphene sheet/film has homogeneous background enclosed with defects with very low conductivity value on its surface. If the defects boundary are considered as smooth the shape and location of defect can be described using truncated Fourier series coefficients. However, it is known that defects (inclusions or void) have very low conductivity value and is used as prior information. In this study instead of estimating the graphene pixel local conductivity distribution, defects geometry and average background conductivity value are estimated. Assuming the defect conductivity be known a priori, the inverse problem here is to estimate the Fourier coefficients that define defects geometry and average background conductivity. In shape

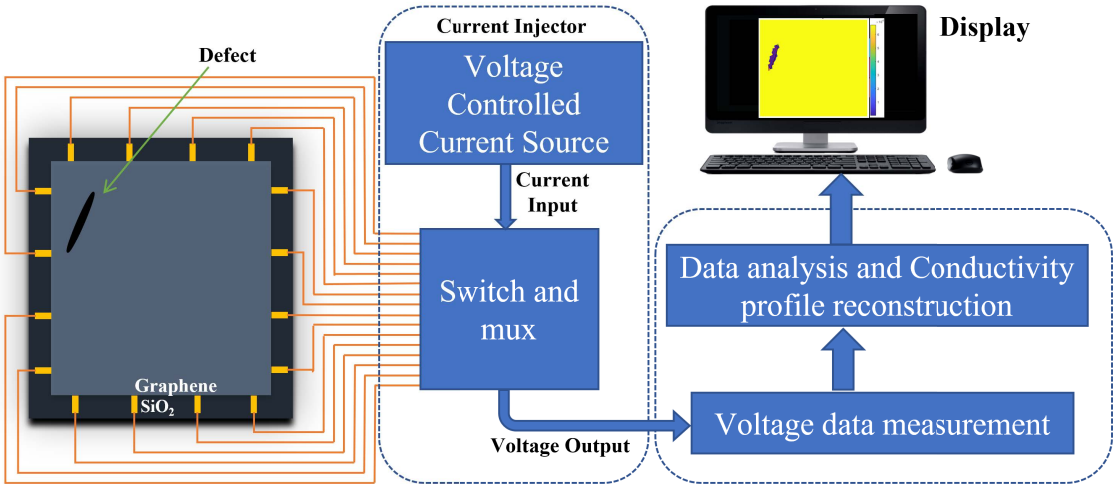

FIGURE 1. Systematic block diagram of EIT for estimating defect location in graphene.

estimation, for complex boundary, higher order Fourier coefficients are used to describe the geometry. Conventional modified Newton Raphson method (mNR) produces intersecting boundaries in case of complex shapes involving higher order Fourier coefficients. In this work we have used PSO-GSA heuristic method which is robust to initial guess and has better estimation performance even with higher order Fourier coefficients. Moreover, PSO-GSA is computationally less intensive as compared to traditional mNR method. Numerical simulations and phantom experiments are performed to estimate the defect boundary and the results are compared against mNR and GSA methods.

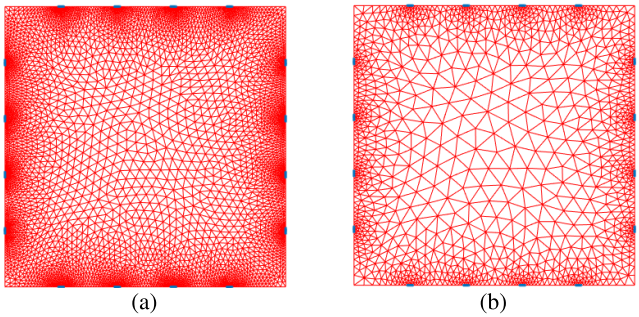

FIGURE 2. Fine and course mesh of graphene used in the study. The boundary electrodes are represented in blue colour attached to the mesh boundary.

II. METHOD

A. NUMERICAL SOLVER AND PHYSICAL MODEL

EIT is a non-invasive imaging method composed of a forward and inverse problem [21]. EIT reconstructs the cross-sectional image of the internal conductivity distribution of the domain. A systematic block diagram of the EIT system for estimating the defect boundary is shown in figure 1. A forward problem in EIT is normally formulated with the finite element method. In forward problem, a constant amplitude current $I_l(l = 1, 2, \cdots, L)$ is applied to the domain Ω understudy and voltage $u(x, y)$ is calculated on the surface electrodes $e_l(l = 1, 2, \cdots, L)$. The calculated voltage $u(x, y)$ and the internal conductivity distribution σ relationship is governed by the Maxwell equation of electromagnetism [22], [23].

$$\nabla \cdot \sigma(P)\nabla u(P) = 0, \quad P = (x, y) \in \Omega \tag{1}$$

To represent a realistic and accurate physical model, a complete electrode model (CEM) is usually used as it takes to account the shunting effect and the contact impedance of the electrodes [24]. Mathematically CEM along with the boundary condition is expressed as

$$u + z_l \sigma \frac{\partial u}{\partial \vec{n}} = V_l, \tag{2}$$

$$\int_{e_l} \sigma(x, y) \frac{\partial u}{\partial \vec{n}} dS = I_l, \quad (x, y) \in e_l \tag{3}$$

$$\sigma(x, y) \frac{\partial u}{\partial \vec{n}} = 0, \quad (x, y) \in \partial\Omega \backslash \bigcup_{l=1}^{L} e_l \tag{4}$$

where $l = (1, 2, \cdots, L)$, z_l is contact impedance between domain surface and electrodes, $\vec{n}$ is the outward unit normal, V_l and I_l is the measured voltage and injected current on l^{th} electrode, respectively. For the existence of a unique solution, Kirchhoff's laws on the measured voltages and injected currents are needed [25], which are defined as

$$\sum_{l=1}^{L} I_l = 0, \quad \sum_{l=1}^{L} V_l = 0 \tag{5}$$

This section describes the mathematical model used in this work. The finite element method (FEM) [26], [27] discretizes the domain into a finite number of triangular elements and each element is assumed to have a constant conductivity

inside itself. Governing equation (1) is numerically solved by FEM. The formulated linear equation of the forward problem is

$$AB = f \tag{6}$$

where A is the stiffness matrix, B is solution vector and f is data vector. The details of the FEM formulation is defined in [21].

B. DEFECT BOUNDARY REPRESENTATION

Let us assume the graphene domain Ω contains a closed and disjoint region (defects) with a smooth boundary $\partial\Omega$ and is assumed to be known. If the boundary of the defects are considered smooth, it can be described by using truncated Fourier series [28] which is defined as

$$Db_n(s) = \begin{pmatrix} x_n(s) \\ y_n(s) \end{pmatrix} = \sum_{f=1}^{F_\phi} \begin{pmatrix} \lambda_f^{x_n} \phi_f^x(s) \\ \lambda_f^{y_n} \phi_f^y(s) \end{pmatrix} \tag{7}$$

where $n = (1, 2, \cdots, N)$, $Db_n(s)$ is the boundary of the n$^{\text{th}}$ object, N is the number of disjoint objects in the domain Ω, F_ϕ is the order of the truncated Fourier series and $\phi_f(s)$ is the basis function which is periodic and represented as

$$\phi_1^\mu(s) = 1 \tag{8}$$

$$\phi_\theta^\mu(s) = \sin\left(2\pi \frac{\theta}{2} s\right), \quad \theta = 2, 4, 6, \cdots, F_\phi - 1 \tag{9}$$

$$\phi_\theta^\mu(s) = \cos\left(2\pi \frac{(\theta - 1)}{2} s\right), \quad \theta = 1, 3, 5, \cdots, F_\phi \tag{10}$$

where $s \in [0, 1]$ and $\mu = x$ or y. The defect boundary can be expressed as shape coefficients (Γ) expressed as

$$\Gamma = (\lambda_1^{\mu_1}, \cdots, \lambda_{F_\phi}^{\mu_1}, \lambda_1^{\mu_N}, \cdots, \lambda_{F_\phi}^{\mu_N})^T \tag{11}$$

C. HYBRID PSOGSA INVERSE SOLVER

In EIT, the inverse problem is a step to calculate the conductivity distribution based on the measured voltages and the injected current. In our case, the inverse problem is the shape estimation and background conductivity of the graphene sheet. The priori information known is the defect conductivity. Here PSOGSA is used to estimate the Fourier series coefficient which defines the defect shape and location on the graphene and the background conductivity of graphene itself.

A population-based hybrid algorithm PSOGSA is the combination of particle swarm optimization (PSO) and gravitational search algorithm (GSA). It is a low-level hybrid algorithm because the functionality of both algorithms i.e. PSO and GSA are combined to run in parallel. The ability of social thinking of PSO is combined with the local search capability of GSA in PSOGSA. To understand the working principle of proposed algorithm, we first need to understand PSO and GSA separately.

Particle swarm optimization (PSO) is based on the social behavior of bird flocking. Each particle (solution candidate) in PSO flies in the search space adjusting its velocity which is influenced by its own and companion's flying experience. These particles are treated as a volume-less particles in the search space. The i^{th} agent in D-dimension is represented in equation (12). The equation also includes the background conductivity of the graphene sheet.

$$\begin{bmatrix} \Gamma_i \\ \sigma_i^b \end{bmatrix} = (\lambda_i^1, \lambda_i^2, \cdots, \lambda_i^D, \lambda_i^b) \tag{12}$$

where σ_i^b is the background conductivity of the graphene sheet and one dimension of the particle defines the conductivity (λ_i^b). The rate of change of position (velocity) of the particle i is updated based on the previous position of the particle i and the position of the best particle among the population. The new position of the particle is according to the previous position and the new velocity, which are mathematically expressed as

$$\begin{aligned} v_i(t) = {} & w \times v_i(t-1) \\ & + c_1 \times rand \times (pbest_i - \begin{bmatrix} \Gamma_i(t-1) \\ \sigma_i^b(t-1) \end{bmatrix}) \\ & + c_2 \times rand \times (gbest - \begin{bmatrix} \Gamma_i(t-1) \\ \sigma_i^b(t-1) \end{bmatrix}) \end{aligned} \tag{13}$$

$$\begin{bmatrix} \Gamma_i(t) \\ \sigma_i^b(t) \end{bmatrix} = \begin{bmatrix} \Gamma_i(t-1) \\ \sigma_i^b(t-1) \end{bmatrix} + v_i(t) \tag{14}$$

where $v_i(t)$ is the velocity of i^{th} particle at t time, w is the weighting function, c_k is a weighting factor, *rand* is random number [0,1], $\Gamma_i(t)$ is the current position of particle i at iteration t, $pbest_i$ is the best particle in that iteration, and *gbest* is the best solution till that iteration. More detailed explanation of PSO can be found in [29].

On the other hand, the gravitational search algorithm (GSA) is based on the law of gravity [30]. The particle is considered objects and their masses are used for measuring their performance. A good particle has a heavier mass and is moved slower than the other masses. The gravitational forces are calculated and based on this force, the velocity acceleration of the particle is updated. The velocity of particle is calculated as

$$v_i(t) = rand_i \times v_i(t-1) + a_i(t-1) \tag{15}$$

where $v_i(t)$ is the velocity, $a_i(t)$ is the acceleration of i^{th} particle at t time. The position of the particle is updated using the equation (14). The detailed explanation can be found in [19].

The ability of social thinking (*gbest*) in PSO is combined with local search capability of GSA to form PSOGSA. Equation (13) and (15) is combined together to mathematically define PSOGSA as

$$\begin{aligned} v_i(t) = {} & w \times v_i(t-1) + C_1' \times rand \times a_i(t-1) \\ & + C_2' \times rand \times (gbest - \begin{bmatrix} \Gamma_i(t-1) \\ \sigma_i^b(t-1) \end{bmatrix}) \end{aligned} \tag{16}$$

where $v_i(t)$ is the velocity of particle i at time t, C_j' is a weighting factor, w is a weighting function, *rand* is a random

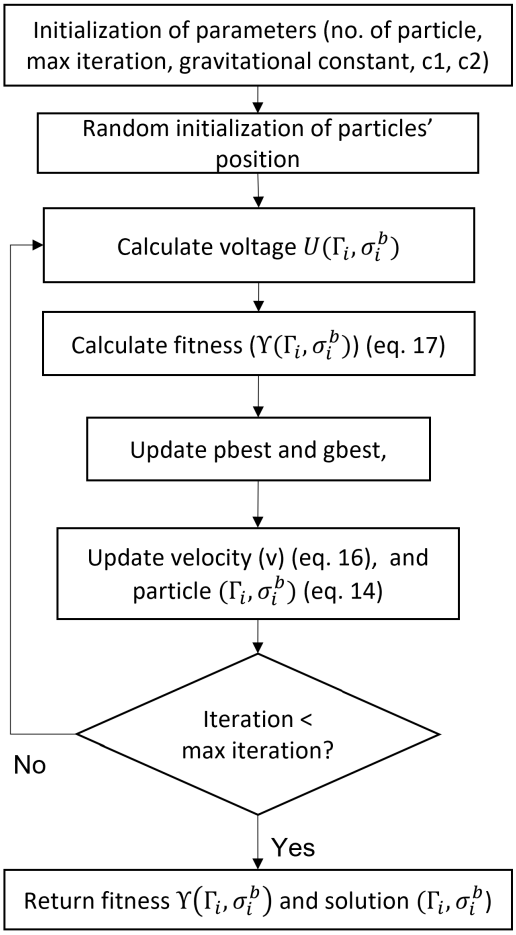

FIGURE 3. Flowchart of the PSOGSA algorithm for estimating defect geometry and the background conductivity of the graphene sheet.

number [0,1], $a_i(t)$ is the acceleration of particle i at time t, and *gbest* is the best particle so far. This updated velocity is used for updating the position of particle for PSOGSA which is defined with equation (14).

The flowchart of PSOGSA for estimating the shape of the defect on the graphene is presented in figure 3. The solutions are updated based on the fitness of each particle, also known as the cost function. The cost function is a function that measures the discrepancy between measured voltages and calculated voltages and is defined as

$$\gamma(\Gamma_i, \sigma_i^b) = \frac{||U(\Gamma_i, \sigma_i^b) - V||^2}{2} \tag{17}$$

where $U(\Gamma_i, \sigma_i^b)$ is the calculated voltage with FEM which depends on the estimated Fourier series coefficients and the background conductivity of the graphene sheet, and V is the measured voltage recorded from the electrical impedance system.

III. RESULT AND DISCUSSION

A numerical simulation and experimental studies are presented in this section in which external defect location and shape on graphene sheet is estimated with PSOGSA. In this study, the conductivity of the graphene sheet is also estimated along with the defect details. The same geometry of the graphene sheet has been used for the numerical and experimental cases and the preparation of the graphene sheet is also described later in the experimental study section. As GSA has good performance in estimating the higher-order Fourier series coefficients in the complex problem of EIT, hence it is used to compare the estimated result from PSOGSA for all the cases. Also mNR, a conventional reconstruction algorithm, is compared against the proposed algorithm. EIDORS [31] framework is used to compute the forward solution of the EIT in the Matlab software. To avoid the inverse crime, two separate mesh is used for the forward and inverse problems which are presented in figure 2. A mesh configured with 9648 elements and 5121 nodes is used in the forward problem, while the mesh in the inverse problem used 2412 elements and 1355 nodes. Both PSOGSA and GSA were configured with the same search space, number of particles, and run for equal iterations. The particles are updated per iteration and the best solution is updated which has a low cost function value.

The robustness of the proposed algorithm is studied with the help of Monte Carlo simulation. In this, each run of PSOGSA is assigned with a different set of particles and a different noise seed. The Monte Carlo simulation is executed only on numerical study for $\eta = 20$ runs for estimating the Fourier series coefficient. The mean value of the Fourier series coefficient is used as the estimated value from the algorithm. Mean ($\bar{\lambda}$) is one of the statistical parameter analyzed by Monte Carlo simulation along with mean absolute error ($\overline{MAE}$), mean error square ($\overline{MES}$), error standard deviation (E_{sd}), and the mean root mean square error ($\overline{RMSE}$). $\overline{MAE}$ and $\overline{RMSE}$ provide the magnitude of estimation error for the corresponding true value. The dispersion of the error (e_i) for estimated parameters is calculated by error standard deviation (E_{sd}) and the square of the bias of the error is given by $\overline{MES}$. The mathematical definition of each parameter are defined below as

$$\bar{\lambda} = \frac{1}{\eta}\sum_{i=1}^{\eta}\lambda_i \tag{18}$$

$$\begin{aligned}\overline{MES} &= \left(\frac{1}{\eta}\sum\nolimits_{i=1}^{\eta}(\lambda_{true} - \lambda_i)\right)^2 \\ &= \left(\frac{1}{\eta}\sum\nolimits_{i=1}^{\eta} e_i\right)^2 = (E[e_i])^2 = (\bar{e})^2\end{aligned} \tag{19}$$

$$\overline{MAE} = \frac{1}{\eta}\sum_{i=1}^{\eta}|\lambda_{true} - \lambda_i| = \frac{1}{\eta}\sum_{i=1}^{\eta}|e_i| \tag{20}$$

$$\begin{aligned}\overline{MSE} &= \frac{1}{\eta}\sum\nolimits_{i=1}^{\eta}(\lambda_{true} - \lambda_i)^2 \\ &= \frac{1}{\eta}\sum\nolimits_{i=1}^{\eta} e_i^2 = E[e_i^2]\end{aligned} \tag{21}$$

$$\begin{aligned}E_{sd} &= \sqrt{\frac{1}{\eta}\sum\nolimits_{i=1}^{\eta}(e_i - \bar{e})^2} \\ &= \sqrt{E[e_i^2] - (E[e_i])^2}\end{aligned}$$

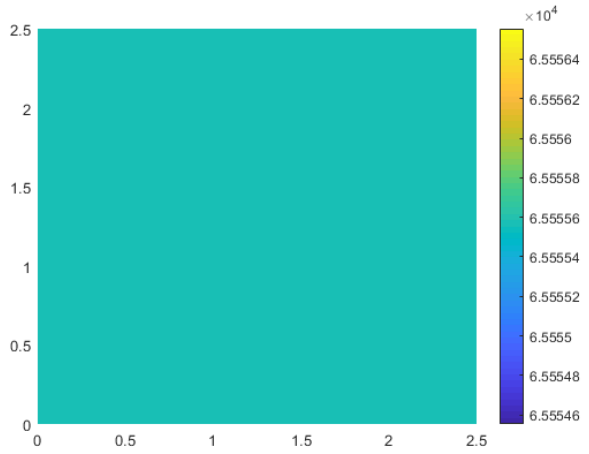

FIGURE 4. Homogeneous case of graphene sheet. The background conductivity is presented by colour bar.

$$= \sqrt{\overline{MSE} - \overline{MES}} \tag{22}$$

$$RMSE = \sqrt{\frac{(\lambda - \lambda_t)^T(\lambda - \lambda_t)}{\lambda_t^T \lambda_t}} \tag{23}$$

$$\overline{RMSE} = \frac{1}{\eta}\sum_{i=1}^{\eta} RMSE_i \tag{24}$$

where λ and λ_t are the estimated and true values of the respective Fourier series coefficients, respectively. The statistical parameters for the numerical cases which are reported which are tabled in a later section that provides the information about the PSOGSA algorithm regarding stability and accuracy. For the boundary estimation of the defect the calculated statistical parameters are $\bar{\lambda}$, $\overline{MAE}$, $\overline{MES}$, and E_{sd}.

A. NUMERICAL STUDY

There are 16 electrodes attached to the boundary of the graphene sample where each side has four electrodes. The conductivity of the background and the defect on the graphene sheet is assumed to be homogeneous and is used as known priori information for estimating the Fourier series coefficient. The defects are resistive to the current flow therefore a very low conductivity value of $5 \times 10^{-9} mS$ is assumed in numerical simulations and of the background to be $6.7 \times 10^4 mS$, respectively. The background conductivity of the graphene sheet is also estimated along with the Fourier series coefficients. A 1% relative white Gaussian noise is added to generated voltage data to account for instrumental and environmental noise.

Initially, a proposed algorithm PSOGSA is used to estimate a homogeneous graphene sheet case for the numerical study. The estimated value of the background conductivity of the graphene sheet is shown figure 4. We can see that the estimated value of conductivity is very close to the true value. A homogeneous graphene sheet sample was used for obtaining the optimum value of contact impedance which has the lowest RMSE of the voltage reading. To optimize the parameters of the proposed algorithm, a test case of single defect on the graphene sheet is considered for estimating defect boundary and the background conductivity of squared shaped domain. The test case with a circular defect is estimated by PSOGSA, see figure 5a. The parameters such as the number of particles is analyzed for both single defect and two defects on the graphene sheet, however, weighting factors and the number of iteration are analyzed only for single defect case using this test case. The weighting factors (C_j') different configuration effect on the performance of the algorithm is initially analyzed. A total of 11 cases of different weighting factors configuration are used (figure 5b) and the corresponding RMSE, and cost function are shown in figure 5c. Out of 11 cases of weighting factors configuration only 3 cases are preferred which have the lower RMSE and cost function compared to other configurations. The 7^{th} configuration of weighting factors gives the low RMSE of a estimated Fourier series coefficients along with a lower cost function. The proposed algorithm performance is compared with different iteration levels. By this analysis, we want to check if there will be any improvement in the performance of the algorithm with more number of iterations. Five different cases for the iteration are presented in the figure 5d. We can see that in almost all cases the cost function converged before 20^{th} iteration and there is no future improvement further. Thus, it is a waste of computational resources to run the PSOGSA algorithm beyond 25^{th} iteration.

The impact of a different number of particles on the PSOGSA estimation is also analyzed. The number of particles is initialized in the range of 20 to 350 with 14 different values. As the number of particles is increased the cost function decreases but the RMSE values are fluctuating after the number of particles is increased beyond 40. The cost function is lower for 5 cases in which the particle size is from 100 to 200, in which RMSE of the Fourier series coefficients is low for 175 particle size. The comparison of the cost function and the RMSE with a different number of particles for the single defect case are presented in figure 5e.

A single defect in the graphene sheet is defined with six Fourier series coefficients which represent a simple shape, i.e., circular and ellipse. Two defects on the graphene sheet are considered to analyze the proposed algorithm for the estimation of the defect boundary. The two defects needed 12 coefficients to define their simple geometry. As the unknowns to be estimated by the proposed algorithm have also doubled in number, we need to increase the number of particles of PSOGSA to achieve the lower cost function. For this two defects scenario, presented in figure 6a, we have analyzed the proposed algorithm with a different particle size. Now the number of particles is in the range of 300 to 1000. The algorithm configured with 600 and 900 particles have shown good result with lower RMSE and cost function. The RMSE of Fourier series coefficient and cost function for the corresponding number of particles are presented in figure 6b. From the figure, we can see that the algorithm configured with 600 particles has a lower cost function and a similar

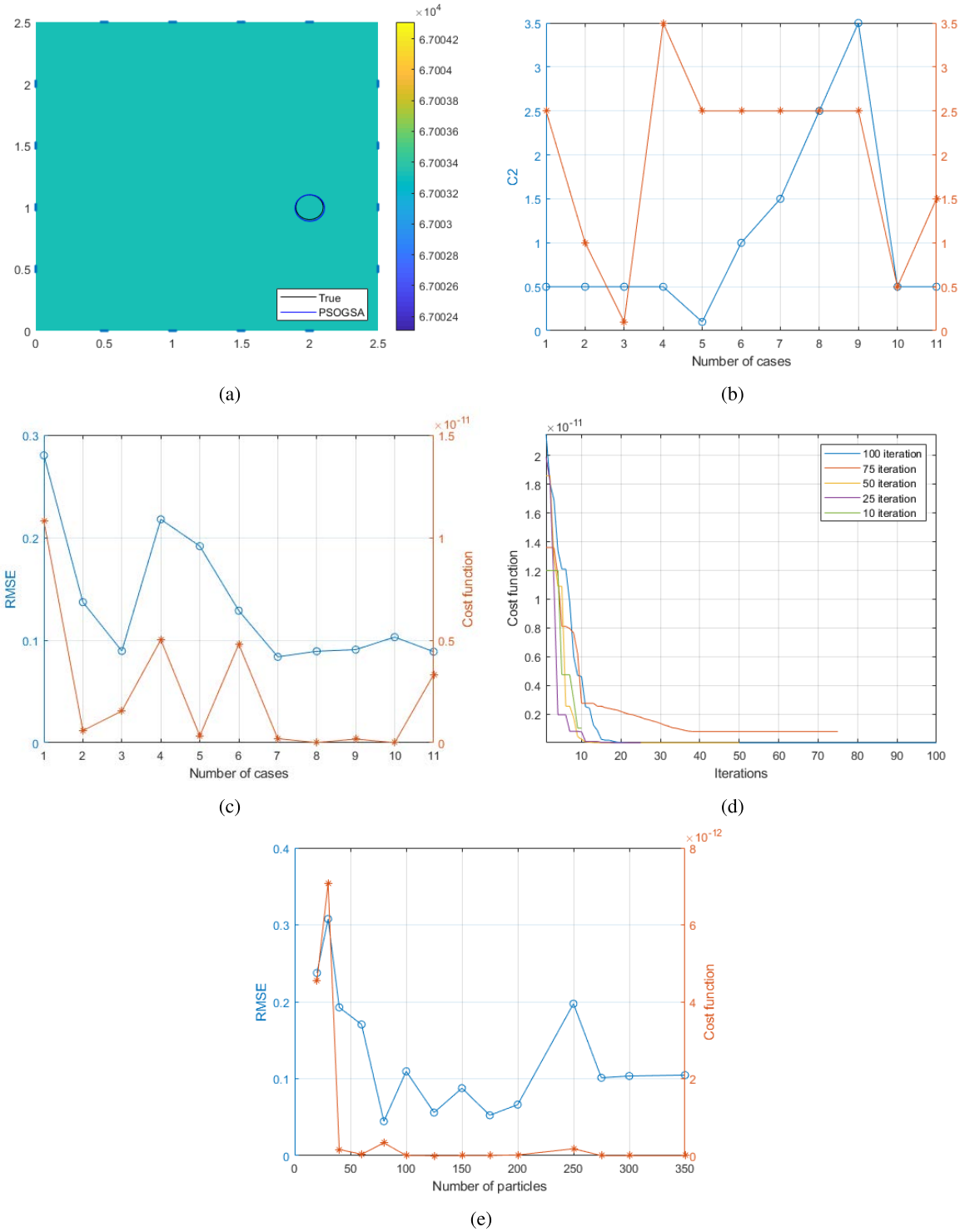

FIGURE 5. Numerical case of single defect on graphene sheet for parameter optimization. (a) True defect location along with the estimated result from PSOGSA. The black circle represent the true and a blue circle represent a estimated location of a defect by PSOGSA. (b) Weighting factors (C_i') combination, (c) RMSE and cost function value for different cases of weighting factor combination, (d) cost function value for a different level of iteration, (e) RMSE and cost function with a different number of particles in PSOGSA.

RMSE of Fourier series coefficient when compared with 900 particles. Since the algorithm configured with the lower number of particles required less computational resources, PSOGSA configured with 600 particles is used to estimate the two defects on the graphene sheet.

An initial guess is required to estimation the defect boundary. PSOGSA and GSA randomly initialized within the search space and for defect boundary estimation, particles are randomly initialized within graphene domain. These particles presents defect with different size at different location which

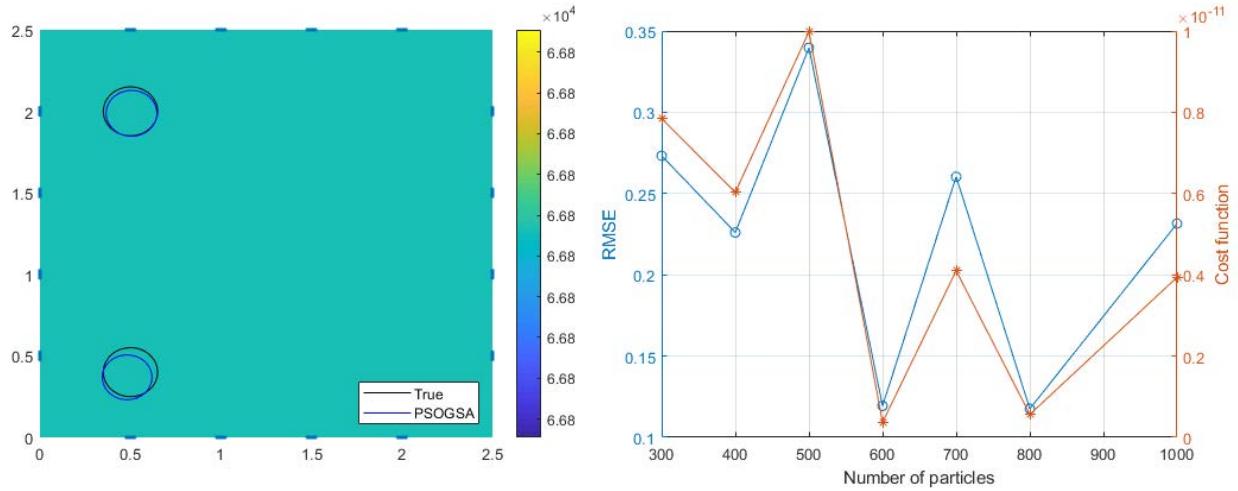

(a) (b)

FIGURE 6. Numerical case of two defects on the graphene sheet for parameter optimization. (a) True defect location along with the estimated result from PSOGSA. The black circle represents the true position of the defect. The estimated location of a defect by PSOGSA is represented by a blue circle. (b)Corresponding RMSE and cost function with a different number of particles in PSOGSA.

are randomly generated with location in range of 0 to 2.5 in both axis. On the other hand, mNR initial guess are close to true boundary which is different for every cases.

A total of 6 cases of a single defect on a graphene sheet are analyzed for estimation of the defect boundary with PSOGSA. In the first case, the defect is located in the lower right corner which is presented in figure 7a. In the figure, we can see that the PSOGSA has estimated the defect location and boundary with good accuracy when compared with the estimation by the GSA and mNR. Similarly in the second case, the defect is located in the top right corner, however, the defect width is very thin when compared to the first case. The second case is presented in figure 7b which also contains the estimation done by all three algorithms. In this case, the estimation of GSA deviated from the true defect location towards the graphene sheet boundary whereas mNR was close to true location but failed to estimate the shape. However, we can see that the defect location estimated by PSOGSA is in close agreement with the true location of the defect. But all algorithm failed to estimated the shape of the defect. In case 3 the single defect is a small size defect when compared with the previous two cases. In this scenario, the defect is located on the lower part of the graphene sheet between 14^{th} and 15^{th} electrodes. This small size defect is harder to estimate but PSOGSA has estimated with a low error which can be seen in the figure 7c along with the estimation result from the GSA and mNR. In these three cases, defects are defined with 6 Fourier series coefficients due to which the shapes are ellipses.

To evaluate the performance of PSOGSA for more complex shapes, defects were defined with more shape coefficients. Eight Fourier coefficients were used to define a single defect on a graphene sheet and were estimated. Cases 4,5, and 6 of single defect with higher Fourier series coefficients are analyzed which are presented in figures 7d, 7e, 7f. We can see that PSOGSA could estimate the defect geometry with good accuracy than other two algorithms. However, when the defect on the graphene sheet is very thin as in figure 7f. PSOGSA estimated defect boundary has same shape as true boundary. PSOGSA presents the estimated result with close location to the true shape whereas estimation done by GSA and mNR diverted from true location.

TABLE 1. RMSE of the estimated Fourier series coefficients by PSOGSA, GSA, and mNR for single defect cases.

Algorithm	Case 1	Case 2	Case 3	Case 4	Case 5	Case 6
PSOGSA	0.0400	0.0757	0.0958	0.2212	0.0475	0.1214
GSA	0.1611	0.1533	0.2303	0.3231	0.2030	0.3085
mNR	0.1466	0.1409	0.1582	0.2664	0.0853	0.7444

All the single defect cases are estimated by the PSOGSA algorithm with a low error than the GSA algorithm. The mNR algorithm failed to estimate the defect boundary in all the single defect cases. From the 6 cases of single defect we can say that the PSOGSA has good performance over the GSA algorithm with the same parameter configurations. The RMSE of the estimated Fourier series coefficients from all three algorithms are presented in table 1. The table of RMSE for Fourier series coefficients shows that PSOGSA has lower RMSE value which suggest better estimation performance.

Two defects on the graphene sheet cases were also studied and the performance of the PSOGSA was evaluated against GSA and mNR. Three different cases are presented for this study. Case 7 is the simplest two defects case study where one defect is on the top left and another one is on the bottom right corner, respectively. The estimation of the defect boundary by PSOGSA is in close agreement with the true geometry

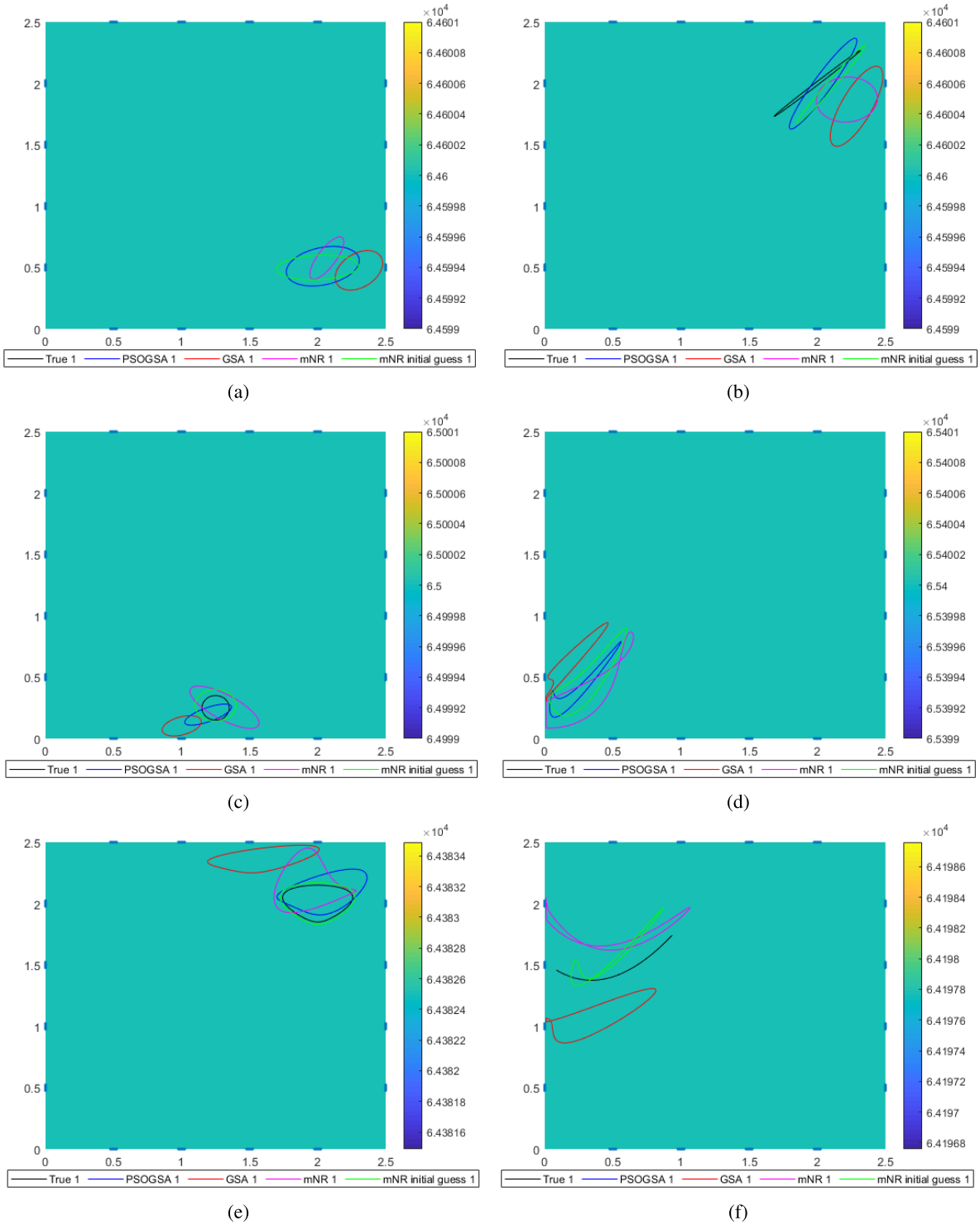

FIGURE 7. Numerical results for cases 1-6,(a-f) with a single defect on graphene surface by PSOGSA, GSA, and mNR. The true location of defect and the initial guess for mNR are presented by a black and green color and the estimated location of a defect by PSOGSA, GSA, and mNR is represented by a blue, red, and magenta color, respectively.

when compared with the estimation result from the GSA and mNR, which is presented in figure 8a. Another two defects scenario on the graphene sheet is labeled as case 8 in which both defects are on the left side of the graphene, seen in figure 8b. In this case, the GSA and mNR estimated the defect location with poor accuracy when compared with PSOGSA. We can see that the PSOGSA has estimated both defects location on the graphene sheet with good accuracy than other

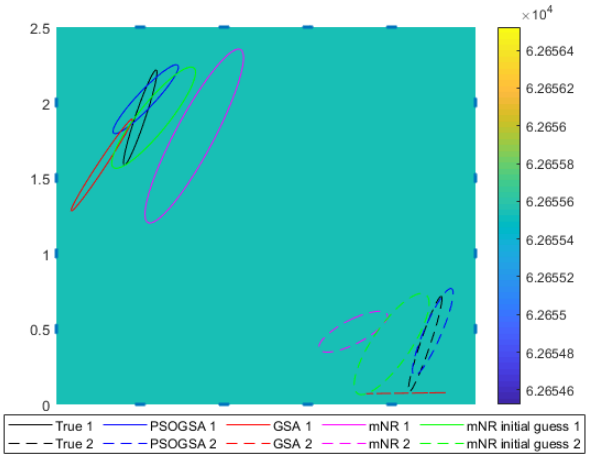

(a)

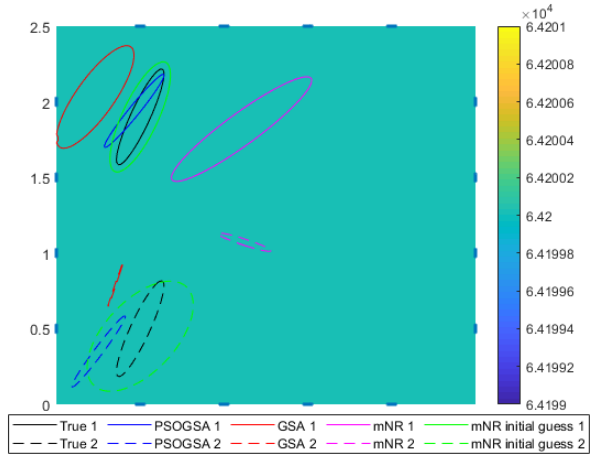

(b)

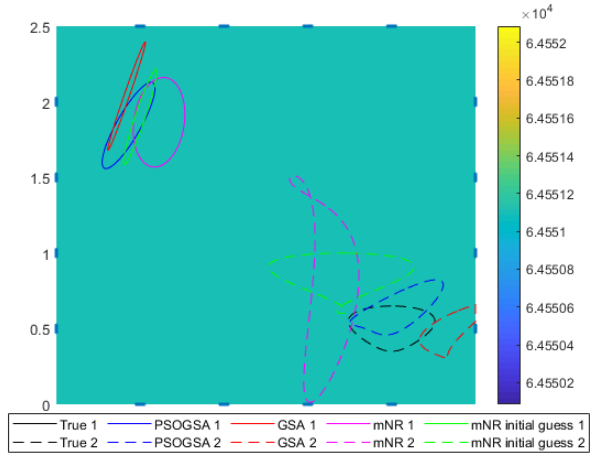

(c)

FIGURE 8. Numerical results for cases 7-9,(a-c) with two defects on graphene surface by PSOGSA, GSA, and mNR. The true location of defect and the initial guess for mNR are presented by a black and green color and the estimated location of a defect by PSOGSA, GSA, and mNR is represented by a blue, red, and magenta color. Defect 1 and 2 are represented by single and dashed line, respectively.

algorithms. In both these cases, i.e. cases 7 and 8, each defect is defined with 6 Fourier series coefficients. To include a complex-shaped defect in case 9 one defect is defined with

TABLE 2. RMSE of the estimated Fourier series coefficients by PSOGSA, GSA, and mNR for two defects cases.

Algo.	Case 7		Case 8		Case 9	
	Defect 1	Defect 2	Defect 1	Defect 2	Defect 1	Defect 2
PSOGSA	0.1252	0.0591	0.0740	0.3936	0.0833	0.0758
GSA	0.2311	0.2319	0.1590	0.5438	0.1280	0.1849
mNR	0.2569	0.2401	0.4582	1.1745	0.1326	0.4730

6 coefficients but another defect is defined with 8 coefficients. In this case, there are now 14 coefficients to be estimated by the algorithms. The true defect geometry along with the estimated geometry of the defects are presented in figure 8c. From the figure, we can see that the PSOGSA could estimate the location of the defect with good accurate than that of GSA, however, mNR failed to estimate the defect boundary. The complex shape of the defect was not estimated with good accuracy. In all cases of two defects scenarios (case 7, 8, and 9), PSOGSA could estimate the geometry of the defect with good accuracy. But GSA failed to estimate the defect location and shape, on the other hand, mNR overestimated the boundary size or presented a intersecting boundary.

Table 2 shows RMSE by all 3 algorithms for the two defects cases. From the table, we can see that in two defects cases PSOGSA has estimated each defect with good accuracy than the estimation done by other two algorithms. Thus, in all 9 numerical cases, PSOGSA estimated the defect on the graphene sheet with good accuracy when compared to GSA and mNR. The standard deviation error of the Fourier series coefficients estimated by PSOGSA is plotted in figure 9. From the figure we can see that it has estimated the coefficients with good accuracy. For most of the cases the first 2 coefficients which defines the location of defect has higher error than other coefficients. Along with the unknown location of the defects in the graphene sheet, the background conductivity is also estimated. The true value of the background is set to $6.7 \times 10^4 mS$ and both algorithms estimated the background conductivity of the graphene sheet. The estimated background conductivity of graphene sheet by PSOGSA is presented along with the estimated result.

B. EXPERIMENTAL STUDY

The EIT system setup used for the experiment consists of a constant current source (Agilent 4284A precision LCR meter) and a data acquisition system (NI PXI-1042Q) to measure the resultant voltage readings.

1) PREPARATION OF GRAPHENE SAMPLE

In this section, a graphene sample on the SiO_2 substrate preparation is explained. A CVD processed graphene sample was purchased from Graphene Square Inc. For a mechanical supporter during the transfer process poly (methylmethacrylate) PMMA (950 PMMA A4) was spin-coated at 300 RPM for 30 seconds on graphene synthesized copper foil and annealed on a hot plate at $100°C$ for 5 minutes.

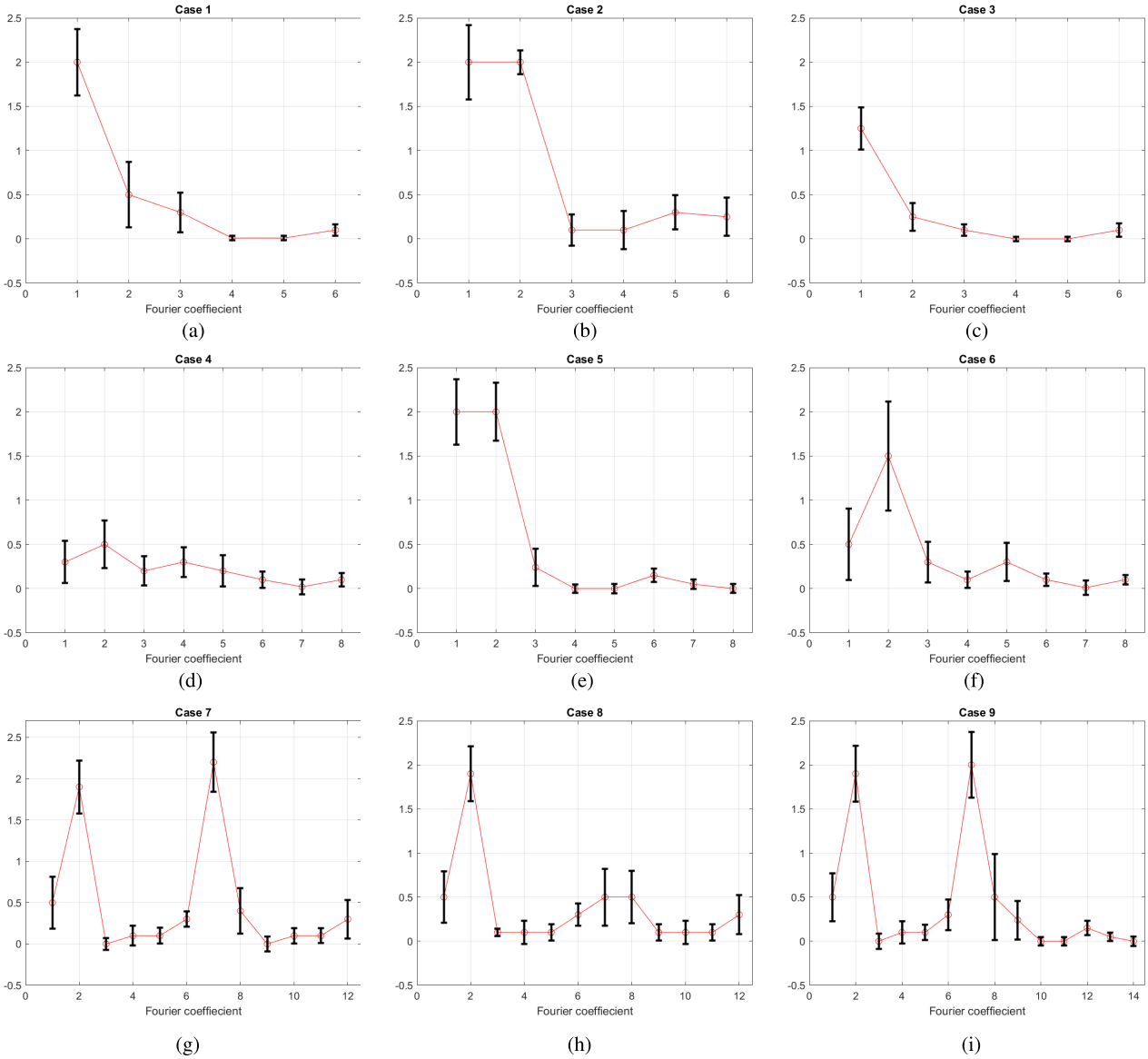

FIGURE 9. Standard deviation error (E_{sd}) of all numerical cases for the estimated Fourier series coefficients by hybrid PSOGSA.

After the supporter is coated, the sample was put into an ammonium persulfate solution to remove the copper foil. PMMA/Graphene was cleaned with deionized water and was later transferred to SiO_2/Si wafer, which is the target substrate used for the experiment, after which PMMA was dissolved using acetone.

A graphene sample of size 2.5 × 2.5 cm is used in this study. A total of 16 copper electrodes are coated on the graphene sample using the sputtering method with a mask which is designed with the electrode location and shape. Each side of the graphene sample has 4 electrodes placed equidistantly and are separated by a gap of 0.5 cm as shown in figure 10. A gold wire, connecting the EIT measurement system to the graphene sample, was attached to the electrodes with the help of silver paste. A current of the constant amplitude of 0.1 mA and frequency of 1KHz is injected into the graphene sheet using a crossed injection pattern. For 16 electrodes setup, a total of 128 voltage measurement reading is obtained from the boundary electrodes.

2) RESULT

Electrode contact impedance can have great influence on reconstruction performance. Especially, in the graphene application, the conductivity is very high so the electrode contact impedance has great effect on measured voltages as compared to other industrial applications such as two-phase flows. Experiment with homogeneous graphene without any defects is carried out and the measured voltages are used to determine the contact impedance of electrodes. From the experiment, the contact impedance of electrodes is obtained

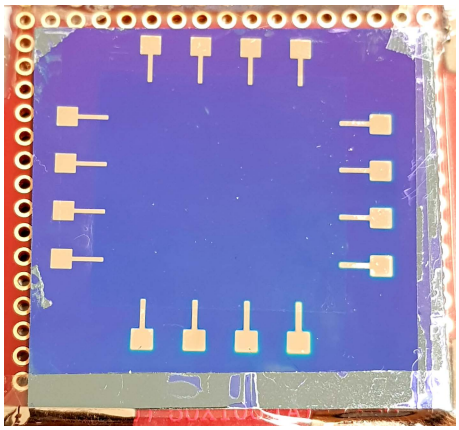

FIGURE 10. Electrode coated graphene sample used for the experimental study.

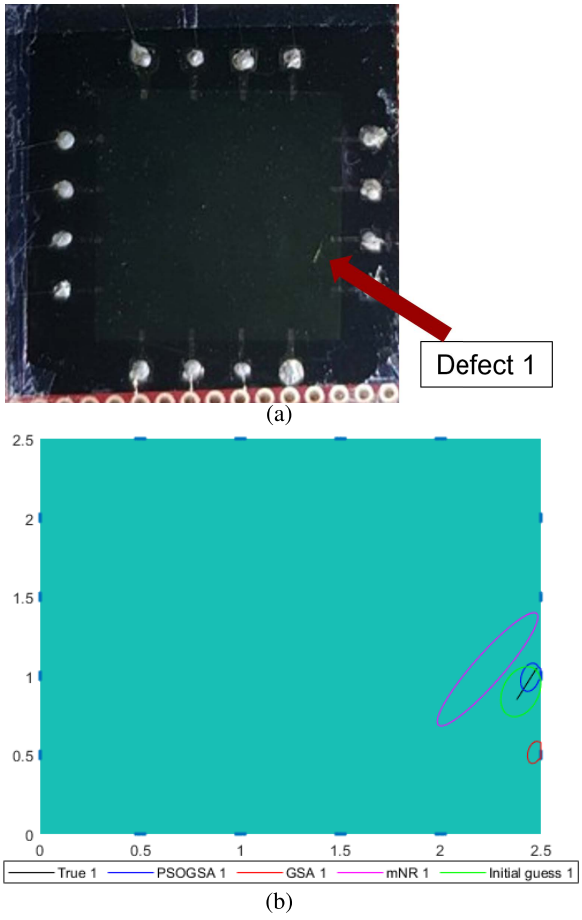

FIGURE 11. Experimental study for case 1 with defect identification on graphene of size 2.5 × 2.5cm. (a) Graphene with a single defect. (b) Experimental result for defect location on the graphene sheet. The initial guess for mNR and the estimated location of a defect by PSOGSA, GSA, and mNR is represented by a green, blue, red, and magenta color, respectively.

as 2.5E-7. A Case of single defect, defect created with a pointed knife, on the surface of a graphene sheet is presented in figure 11a where we can see the defect is located near 7th electrode. For estimating this single defect scenario,

TABLE 3. Estimated conductivity (*mS*) of graphene sheet by PSOGSA and GSA.

Case	PSOGSA	GSA
Single defect	6.25×10^4	6.58×10^4
Two defects	6.68×10^4	6.1×10^4

PSOGSA is configured with 450 particles and iterated for 25 iterations. Figure 12a presents a true scenario where two defects are present on a graphene sheet. In this scenario, one defect is located on the lower right side of the graphene sheet near the 7th electrode and the second defect is located on the top side of the sample near 3rd electrode. Both defects are made with a pointed knife on the surface of the graphene sheet. The presence of two defects has increased the number of unknown parameters to be estimated. As the number of unknowns is increased, thus the number of particles in the algorithm is increased to 750 for better estimation results.

Figure 11b shows the estimated result of the single defect location by all algorithms together with the true location. We can see that the estimated location of the single defect by PSOGSA is in close agreement with the true location whereas the estimated location by GSA is far away from the true location. The estimated location of defects for the second experiment case of two defects on graphene is presented in figure 12b. In this, we can see that the PSOGSA has estimated the location of both defects successfully with good accuracy whereas GSA could only estimate one defect location with good accuracy but failed to estimate the 2nd defect on graphene. The estimation of defects by mNR in both experimental cases overestimated the defect geometry. The small size of defect is not estimated by mNR. Also, the background conductivity of graphene is estimated for both experimental cases along with defect location. The estimated background conductivity of the graphene sheet can be seen in table 3. The mNR algorithm only estimated the Fourier series coefficients whereas GSA and PSOGSA estimated background conductivity of graphene sheet along with Fourier series coefficients.

From both the numerical and experimental studies, we see that the PSOGSA performed better in all the scenarios when compared with GSA and mNR. The proposed algorithm PSOGSA estimated conductivity of the graphene sheet along with the defect geometry. The conductivity of graphene sheet highly depends defect's geometry due to which each case has different background conductivity. Moreover, the proposed algorithm PSOGSA estimated the parameters of two different search space, i.e., Fourier series coefficient and background conductivity but the other inverse algorithm only estimated in single search space. In the complex situation presented in all the cases, PSOGSA has a very good estimation result with good accuracy for estimating the Fourier series coefficients than GSA. However, for achieving more accurate result the particle size of the algorithm is increased but this will increase the computational cost. All the three algorithms have the computational cost which was studied. We have compared

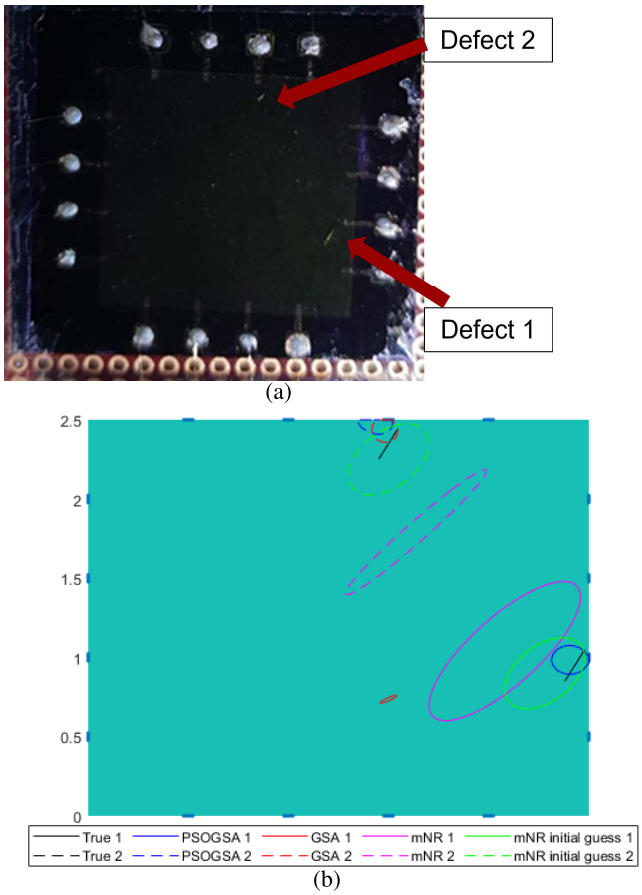

FIGURE 12. Experimental study for case 2 with defects identification on graphene of size 2.5 × 2.5cm. (a) Graphene with two defects. (b) Experimental result for defect location on the graphene sheet. The initial guess for mNR and the estimated location of a defect by PSOGSA, GSA, and mNR is represented by a green, blue, red, and magenta color and defect 1 and 2 are represented by single and dashed line, respectively.

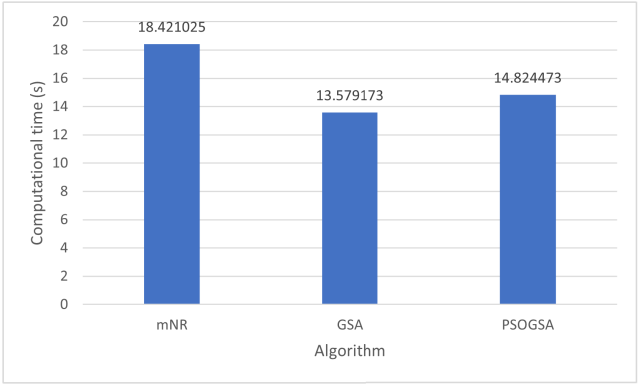

FIGURE 13. Time required by the algorithms for executing a single iteration.

the time required by these algorithms for executing a single iteration. Graph in figure 13 represents the computational time for single iteration of all algorithms. From the graph we can see that mNR required more time due to the Jacobian matrix calculation. GSA and PSOGSA used same particle size for the computational and we can see PSOGSA takes little more time than GSA but the estimation result of PSOGSA is better. Thus, a trade-off between estimation accuracy and computational cost is the major factor when tuning the proposed algorithm. To overcome this issue we have checked the proposed algorithm with different particle size and have used the minimum particle which gives the lowest RMSE value.

IV. CONCLUSION

In this study, electrical characterization of graphene is achieved by estimating the defect location and background conductivity using electrical resistance tomography. The defect boundaries are assumed to be smooth and are described using truncated Fourier series coefficients. The unknown Fourier coefficients and background conductivity are estimated using particle swarm optimization-gravitational search algorithm (PSOGSA). The performance of PSOGSA is analyzed with different numerical cases for single and multiple defects. The effect of different parameter configurations (weighting factors, particle size, and total iteration) on PSOGSA is analyzed. Based on this analysis the initial conditions of PSOGSA are configured for better performance and the iteration size is configured to 25 step. Particle size of PSOGSA depends on the number of parameters that are to be estimated. For single defect case, PSOGSA with 175 particles has the best reconstruction performance and for two defects, 600 particles are used.

Monte Carlo simulation with different noise seed is done for analyzing the statistical parameters which verifies the robustness of the proposed algorithm. Statistical analysis is carried out for all numerical cases and it is seen that PSOGSA could estimate Fourier coefficients corresponding to the shape of the defect with great accuracy as compared to location. This is reflected by the standard deviation error of the Fourier coefficients. In all the numerical cases, PSOGSA estimated background conductivity and defects geometry with good accuracy. However, in the two defects numerical cases involving complex defect shape, mNR and GSA failed to estimate the defect location and shape. In the experimental study PSOGSA has estimated defect with good accuracy whereas GSA and mNR failed to estimate the defect location. Also, in both experimental cases PSOGSA estimated graphene sheet conductivity with less error deviation when compared with GSA.

A better estimation result is obtained from the PSOGSA because it has the exploration capability from PSO, which makes it better than GSA. Due to complex Jacobian matrix calculation in mNR, it tends to produce intersecting boundaries for complex defect shape. However, PSOGSA is free from the Jacobian matrix calculation and is able to estimate the boundary of a complex shape. Also, PSOGSA estimated parameters belonging to two separate search space (Fourier coefficients and background conductivity), however mNR only estimated parameters of a single search space. GSA was also used to estimate the parameters of two separate search space but the estimation error was higher than PSOGSA using the same algorithm parameters. The main drawback of the

PSOGSA is the computational cost which increases with the increase in the particle size and the number of unknowns.

REFERENCES

[1] K. I. Bolotin, K. J. Sikes, Z. Jiang, M. Klima, G. Fudenberg, J. Hone, P. Kim, and H. Stormer, "Ultrahigh electron mobility in suspended graphene," *Solid State Commun.*, vol. 146, pp. 351–355, Jun. 2008.

[2] J.-N. Fuchs and M. O. Goerbig, "Introduction to the physical properties of graphene," *Lect. Notes*, vol. 10, pp. 11–12, 2008. [Online]. Available: https://web.physics.ucsb.edu/~phys123B/w2015/pdf_CoursGraphene2008.pdf

[3] B. Jayasena and S. Subbiah, "A novel mechanical cleavage method for synthesizing few-layer graphenes," *Nanosc. Res. Lett.*, vol. 6, no. 1, pp. 1–7, Dec. 2011.

[4] M. Jin, H.-K. Jeong, T.-H. Kim, K. P. So, Y. Cui, W. J. Yu, E. J. Ra, and Y. H. Lee, "Synthesis and systematic characterization of functionalized graphene sheets generated by thermal exfoliation at low temperature," *J. Phys. D, Appl. Phys.*, vol. 43, no. 27, Jul. 2010, Art. no. 275402.

[5] N.-W. Pu, C.-A. Wang, Y. Sung, Y.-M. Liu, and M.-D. Ger, "Production of few-layer graphene by supercritical CO_2 exfoliation of graphite," *Mater. Lett.*, vol. 63, no. 23, pp. 1987–1989, Sep. 2009.

[6] A. Reina, X. Jia, J. Ho, D. Nezich, H. Son, V. Bulovic, M. S. Dresselhaus, and J. Kong, "Large area, few-layer graphene films on arbitrary substrates by chemical vapor deposition," *Nano Lett.*, vol. 9, no. 1, pp. 30–35, 2008.

[7] X. Liang, B. A. Sperling, I. Calizo, G. Cheng, C. A. Hacker, Q. Zhang, Y. Obeng, K. Yan, H. Peng, Q. Li, and X. Zhu, "Toward clean and crackless transfer of graphene," *ACS Nano*, vol. 5, no. 11, pp. 9144–9153, 2011.

[8] A. Cultrera, D. Serazio, A. Zurutuza, A. Centeno, O. Txoperena, D. Etayo, A. Cordon, A. Redo-Sanchez, I. Arnedo, M. Ortolano, and L. Callegaro, "Mapping the conductivity of graphene with electrical resistance tomography," *Sci. Rep.*, vol. 9, no. 1, pp. 1–9, Dec. 2019.

[9] A. K. Khambampati, S. A. Rahman, S. K. Sharma, W. Y. Kim, and K. Y. Kim, "Imaging conductivity changes in monolayer graphene using electrical impedance tomography," *Micromachines*, vol. 11, no. 12, p. 1074, Dec. 2020.

[10] A. K. Khambampati, S. A. Rahman, S. K. Sharma, W. Y. Kim, and K. Y. Kim, "Nonlinear difference imaging to image local conductivity of single-layer graphene using electrical impedance tomography," *IEEE Trans. Instrum. Meas.*, vol. 71, pp. 1–12, 2022.

[11] S. K. Sharma, S. K. Konki, A. K. Khambampati, and K. Y. Kim, "Bladder boundary estimation by gravitational search algorithm using electrical impedance tomography," *IEEE Trans. Instrum. Meas.*, vol. 69, no. 12, pp. 9657–9667, Dec. 2020.

[12] D. Liu, A. K. Khambampati, S. Kim, and K. Y. Kim, "Multi-phase flow monitoring with electrical impedance tomography using level set based method," *Nucl. Eng. Des.*, vol. 289, pp. 108–116, Aug. 2015.

[13] S. Kim, U. Z. Ijaz, A. K. Khambampati, K. Y. Kim, M. C. Kim, and S. I. Chung, "Moving interfacial boundary estimation in stratified flow of two immiscible liquids using electrical resistance tomography," *Meas. Sci. Technol.*, vol. 18, no. 5, p. 1257, 2007.

[14] D. Liu, D. Gu, D. Smyl, J. Deng, and J. Du, "B-spline-based sharp feature preserving shape reconstruction approach for electrical impedance tomography," *IEEE Trans. Med. Imag.*, vol. 38, no. 11, pp. 2533–2544, Nov. 2019.

[15] D. Gu, D. Liu, D. Smyl, J. Deng, and J. Du, "Supershape recovery from electrical impedance tomography data," *IEEE Trans. Instrum. Meas.*, vol. 70, pp. 1–11, 2021.

[16] Y. Li, L. Rao, R. He, G. Xu, Q. Wu, W. Yan, G. Dong, and Q. Yang, "A novel combination method of electrical impedance tomography inverse problem for brain imaging," *IEEE Trans. Magn.*, vol. 41, no. 5, pp. 1848–1851, May 2005.

[17] S. K. Konki, A. K. Khambampati, S. K. Sharma, and K. Y. Kim, "A deep neural network for estimating the bladder boundary using electrical impedance tomography," *Physiolog. Meas.*, vol. 41, no. 11, Nov. 2020, Art. no. 115003.

[18] U. Z. Ijaz, A. K. Khambampati, M. C. Kim, S. Kim, J. S. Lee, and K. Y. Kim, "Particle swarm optimization technique for elliptic region boundary estimation in electrical impedance tomography," in *Proc. AIP Conf.* College Park, MD, USA: American Institute of Physics, 2007, pp. 896–901.

[19] E. Rashedi, H. Nezamabadi-Pour, and S. Saryazdi, "GSA: A gravitational search algorithm," *J. Inf. Sci.*, vol. 179, no. 13, pp. 2232–2248, 2009.

[20] S. Mirjalili and S. Z. M. Hashim, "A new hybrid PSOGSA algorithm for function optimization," in *Proc. Int. Conf. Comput. Inf. Appl.*, Dec. 2010, pp. 374–377.

[21] M. Vauhkonen, "Electrical impedance tomography and prior information," Ph.D. thesis. Univ. Kuopio, Kuopio, Finland, 1997.

[22] J. G. Webster, Ed., *Electrical Impedance Tomography*, Bristol, U.K.: Adam Hilger, 1990.

[23] D. S. Holder, "Electrical impedance tomography (EIT) of brain function," *Brain Topography*, vol. 5, no. 2, pp. 87–93, 1992.

[24] K.-S. Cheng, D. Isaacson, J. C. Newell, and D. G. Gisser, "Electrode models for electric current computed tomography," *IEEE Trans. Biomed. Eng.*, vol. 36, no. 9, pp. 918–924, Sep. 1989.

[25] E. Somersalo, M. Cheney, and D. Isaacson, "Existence and uniqueness for electrode models for electric current computed tomography," *SIAM J. Appl. Math.*, vol. 52, no. 4, pp. 1023–1040, Jul. 1992.

[26] S. Brenner and R. Scott, *The Mathematical Theory of Finite Element Methods*, vol. 15. Berlin, Germany: Springer, 2007.

[27] O. C. Zienkiewicz and R. L. Taylor, *Finite Element Method*, vol. 3. Amsterdam, The Netherlands: Elsevier, 2000.

[28] V. Kolehmainen, A. Voutilainen, and J. P. Kaipio, "Estimation of non-stationary region boundaries in EIT—State estimation approach," *Inverse Problems*, vol. 17, no. 6, p. 1937, 2001.

[29] Y. Shi and R. C. Eberhart, "Empirical study of particle swarm optimization," in *Proc. Congr. Evol. Comput. (CEC)*, vol. 3, Jan. 2003, pp. 1945–1950.

[30] B. Schutz, *Gravity From the Ground Up: An Introductory Guide to Gravity and General Relativity*. Cambridge, U.K.: Cambridge Univ. Press, 2003.

[31] A. Adler and W. R. B. Lionheart, "Uses and abuses of EIDORS: An extensible software base for EIT," *Physiolog. Meas.*, vol. 27, no. 5, pp. 25–42, May 2006.

SUNAM KUMAR SHARMA received the B.E. degree in electronics and communication engineering from Pokhara University, Nepal, in 2006, and the M.S. degree in information technology from Sikkim Manipal University, India, in 2016. He is currently pursuing the Ph.D. degree in electronic engineering with Jeju National University, Jeju, South Korea. His research interests include inverse problems, subsurface resistivity, deep learning, and electrical impedance tomography.

ANIL KUMAR KHAMBAMPATI received the B.S. degree in mechanical engineering from Jawaharlal Nehru Technological University, India, in 2003, and the M.S. degree in marine instrumentation engineering and the Ph.D. degree in electronic engineering from Jeju National University, South Korea, in 2006 and 2010, respectively. Since 2010, he has been a Postdoctoral Fellow with the Department of Electronic Engineering, Jeju National University. His current research interests include estimation theory, inverse problems, intelligent fault detection and diagnosis, instrumentation and control, and electrical impedance tomography.

KYUNG YOUN KIM received the B.S., M.S., and Ph.D. degrees in electronic engineering from Kyungpook National University, Daegu, South Korea, in 1983, 1986, and 1990, respectively. From 1994 to 1995, he was a Post-doctoral Fellow with the Department of Electrical Engineering, University of Maryland at Baltimore County (UMBC), Baltimore, MD, USA. From 2001 to 2002, he was a Visiting Professor with the Department of Applied Physics, Kuopio University, Kuopio, Finland. Since 1990, he has been with the Department of Electronic Engineering, Jeju National University, Jeju, South Korea, where he is currently a Professor. Since 2004, he has been a Visiting Professor with the Department of Biomedical Engineering, Rensselaer Polytechnic Institute (RPI), Troy, NY, USA. His current research interests include estimation theory, inverse problems, intelligent fault detection and diagnosis, instrumentation and control, and electrical impedance tomography.